SEMIANNUAL STATUS REPORT
(Millimeter-Wavelengths Propagation Studies)
November 1971 through April 1972

D.B. Hodge and L.R. Zintsmaster

The Ohio State University

ElectroScience Laboratory

Department of Electrical Engineering
Columbus, Ohio 43212

Semiannual Status Report 2374-9
May 1972

Grant Number NGR 36-008-080

National Aeronautics and Space Administration
Office of Grants and Research Contracts
Washington, D.C. 20546

NOTICES

REPORT
by
THE OHIO STATE UNIVERSITY ELECTROSCIENCE LABORATORY
COLUMBUS, OHIO 43212

Sponsor	National Aeronautics and Space Administration Office of Grants and Research Contracts Washington, D.C. 20546
Grant Number	NGR 36-008-080
Investigation of	Millimeter-Wavelengths Propagation Studies
Subject of Report	Semiannual Status Report November 1971 through April 1972
Submitted by	D.B. Hodge and L.R. Zintsmaster ElectroScience Laboratory Department of Electrical Engineering The Ohio State University
Date	May 1972

INTRODUCTION

This report summarizes the experimental and theoretical effort completed during the current time period in conjunction with the ATS-5 Millimeter Wave Experiment. The body of the report consists of two papers which were presented at the 1972 USNC-URSI Spring Meeting, Washington, D.C., April 14, 1972; these papers summarize the experimental and theoretical efforts conducted under this grant, respectively.

During 1970 and 1971 attenuation, radiometric temperature, and rain rate data were obtained by The Ohio State University in conjunction with ATS-5 15.3 GHz downlink measurements. These data were gathered at two ground receiving terminals spaced 4 km apart during 1970 and 8 km apart during 1971. These data have been subsequently analyzed to determine the space diversity characteristics of this communications link. The results of this analysis indicate that substantial improvements in system performance may be gained through the use of space diversity.

In a parallel effort a simple, tractable thunderstorm cell model has been examined to determine its utility in estimating the long term fading statistics of both single terminal and two terminal diversity systems. The model was designed to incorporate readily available U.S. Weather Service rain statistics; thus, the resulting predictions are geographically dependent upon each particular terminal location. Using this simple cylindrical storm cell model, the resulting predictions agreed with experimental ATS-5 measurements within a range of 3 dB.

THE USE OF SPACE DIVERSITY IN THE RECEPTION OF MILLIMETER WAVELENGTH SATELLITE SIGNALS

D.B. Hodge

ABSTRACT

The various meteorolgical parameters that influence millimeter wavelength satellite-to-ground space diversity links are summarized. Space diversity propagation statistics obtained using the 15.3 GHz down-link on ATS-5 are presented. These results include comparison of data obtained using site separations of 4 and 8 km. Propagation data were recorded at Columbus, Ohio, during 1970 using a site separation of 4 km and during 1971 using a site separation of 8 km. The radiometric temperature as well as attenuation of the satellite signal was recorded in both cases for correlation purposes. Both statistics of individual storm events and cumulative statistics have been analyzed yielding single site and joint fade distributions, correlation between attentuation experienced at the two receiving terminals, and correlation between path radiometric temperatures observed at the two receiving terminals. These data indicate that the use of space diversity is indeed effective in improving the reliability of millimeter wavelength satellite-to-ground communication links.

It has been well established that fade depths exceeding typical system margins may be encountered for significant periods of time on millimeter wavelength earth-satellite links. These deep fades are a result of intense rain rates associated with thunderstorm cells located along the propagation path. Unfortunately, the occurrence of thunderstorms is not uniformly distributed throughout the year. For example, in Ohio thunderstorms and intense rains are much more likely to occur during the months of May, June, and July. In addition, the occurrence of thunderstorms is not uniformly distributed throughout the day, their occurrence being more likely in the late afternoon and early evening hours. Thus we may conclude that fade distributions and reliability statistics expressed on an annual basis will be rather optimistic during the thunderstorm season and even during certain hours of the day.

In order to improve the reliability of these systems, the use of space diversity in the reception of the satellite signals has been proposed. This approach takes advantage of the fact that most of the deep fades are a result of high rain rates associated with intense thunderstorm cells. These thunderstorm cells are, in turn, quite limited in horizontal extent as compared with showers having lower rain rates, which may be rather widespread horizontally. Obviously, both types of rain are limited in vertical extent. An example of a single thunderstorm cell is shown in the PPI radar photograph in Fig. 1. This cell was observed on June 14, 1971, using a 15 GHz radar system. The antenna elevation was 7°, the azimuth ranges from 240° to 330°, and the range marks are at two mile intervals. The finite extent of the cell and the irregular shape should be noted in particular. A second PPI photograph of this cell, taken a few minutes later, is shown in Fig. 2. In this case the radar was being operated in a contour mode such that areas producing large reflected signals are blanked out. Here we note that the highly reflective area associated with intense rain is further concentrated within the cell itself. Thus, the space diversity technique takes advantage of the limited extent of intense rains by utilizing two receiving terminals, one of which is intended to "look" around or over the cell while the other is experiencing a fade. It is evident that the statistical properties of the cell shape, extent, orientation, and height, as well as the rain rate distribution within the cell, will ultimately determine the optimum separation distance and direction of the receiving terminals and the resulting improvement of system performance. Further complicating this problem is the fact that these controlling cell characteristics are dependent on the climatological region; and, thus, the optimum diversity configuration and resulting system improvement will vary throughout the United States.

Figures 3 and 4 show worst and best case examples, respectively, of three terminal space diversity data provided by Dr. D.C. Hogg, Bell Telephone Laboratories, Inc. The time delay between the occurrence of maximum attenuation at the different terminals varies from a few minutes to almost an hour. Nevertheless, some diversity improvement would result in each case.

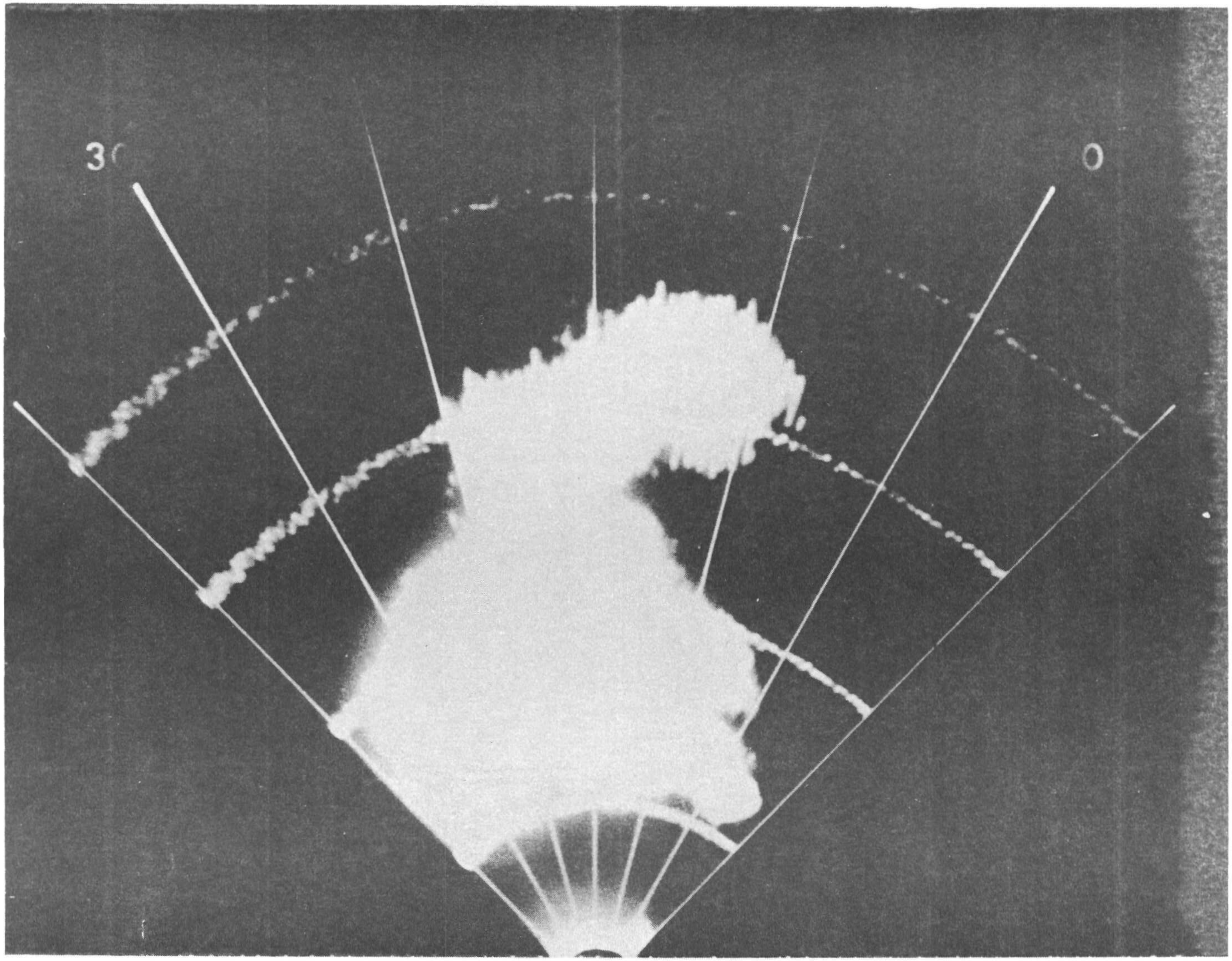

Fig. 1. PPI display of thunderstorm cell (range marks at 2 mile intervals).

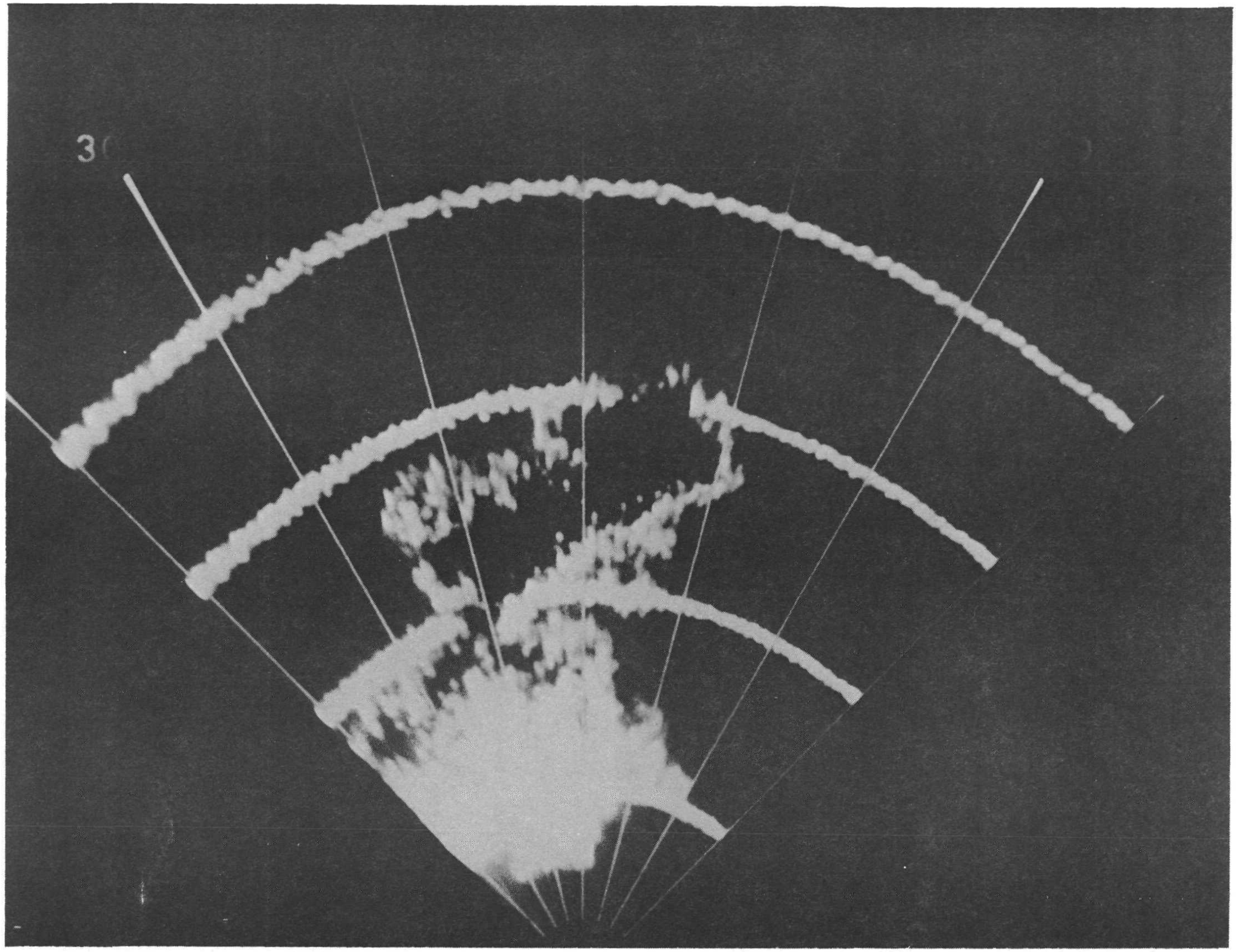

Fig. 2. Contour display of cell shown in Fig. 1.

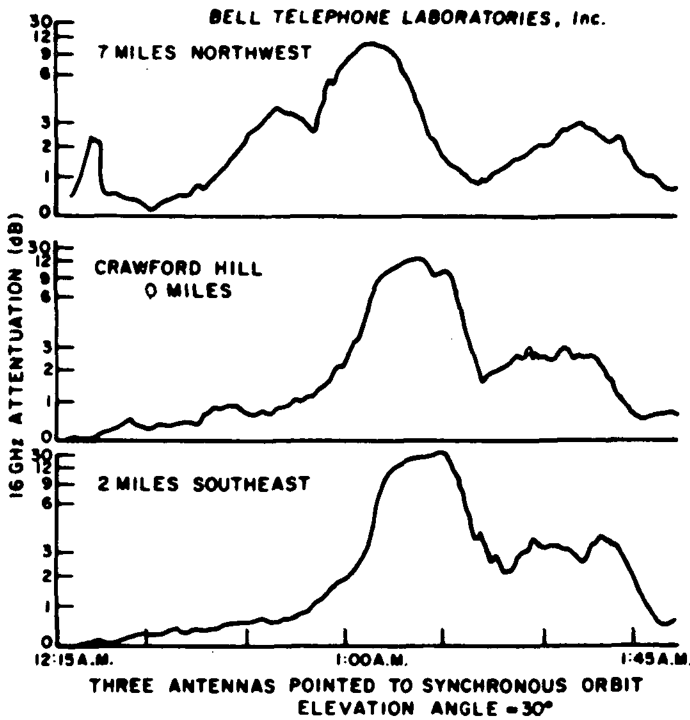

Fig. 3. Three terminal diversity--
worst case example.

Space diversity measurements were made by the Ohio State University, Columbus, Ohio, using the ATS-5 15.3 GHz down-link during 1970 and 1971. The terminal separation distance was approximately 4 km during the 1970 data period and 8 km during the 1971 data period. The initial spacing of 4 km was chosen because available rain distribution data [1] indicated that the cross-correlation between the fading observed at two terminals separated by this distance would be on the order of 0.5. Although this is not a desirable criterion for the establishment of a practical diversity system, it was felt that this approach would yield information concerning the dependence of correlation upon the site separation distance more rapidly than the choice of very large or small separation distances for the initial experiment. In addition, the direction of site separation was oblique with respect to the propagation paths rather than perpendicular to them in order to achieve vertical as well as horizontal separation between the two paths. The top and side views of the site locations are shown in Figs. 5 and 6.

During the 1970 data period a 30 foot parabolic antenna was used at the fixed terminal and a 15 foot parabolic antenna was used at the transportable terminal, site 1. These antennas are shown in Fig. 7 along with the transportable equipment van which may be seen to the

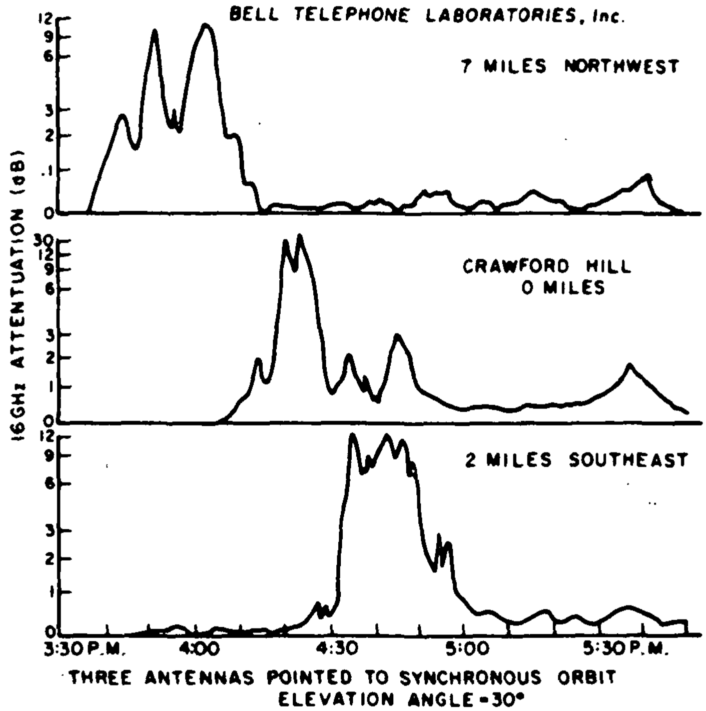

Fig. 4. Three terminal diversity--
best case example.

right of the smaller antenna. Since the 30 foot antenna was not designed for operation in high wind speed environments, such as those encountered during the passage of severe thunderstorms, it was replaced by a new 15 foot antenna before the start of the 1971 data period. No significant reduction in system margin was incurred with this change since the gain of the original 30 foot antenna at this frequency was limited by surface roughness to approximately the same gain as the smaller, new antenna. Square, corrugated feed horns having equal E- and H-plane patterns were used to illuminate these antennas; the two orthogonal linearly polarized components were then fed, respectively, to the PLL receiver and the radiometer. The remaining instrumentation has been described in References 2,3, and 4.

A sample of the raw data obtained using the 4 km separation distance during 1970 is shown in Fig. 8. The upper trace in each case gives the radiometric temperature measured along the propagation path and the lower trace is the pulse-by-pulse record of the received coherent signal. At approximately 1000 Z a small, rather intense thunderstorm cell passed through the propagation paths producing very rapid, deep fades. The fade depth at the fixed terminal was in excess of 12 dB, while the fade depth at the transportable terminal was approximately 6 dB. The maximum cross-correlation between the signals received at the two terminals was associated with a time delay of 8 minutes. The

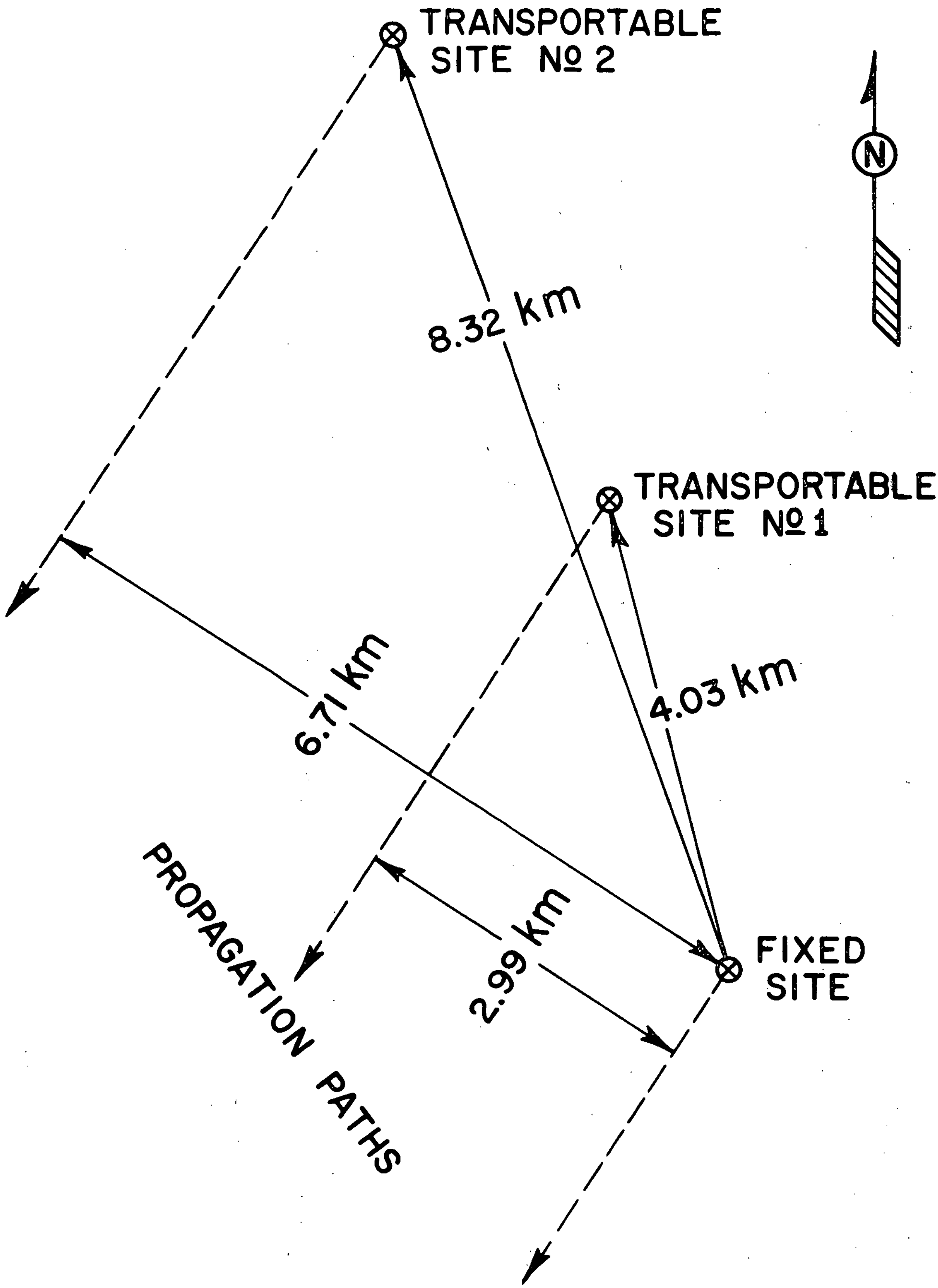

Fig. 5. Top view of site locations.

SIDE VIEW OF PROPAGATION PATHS

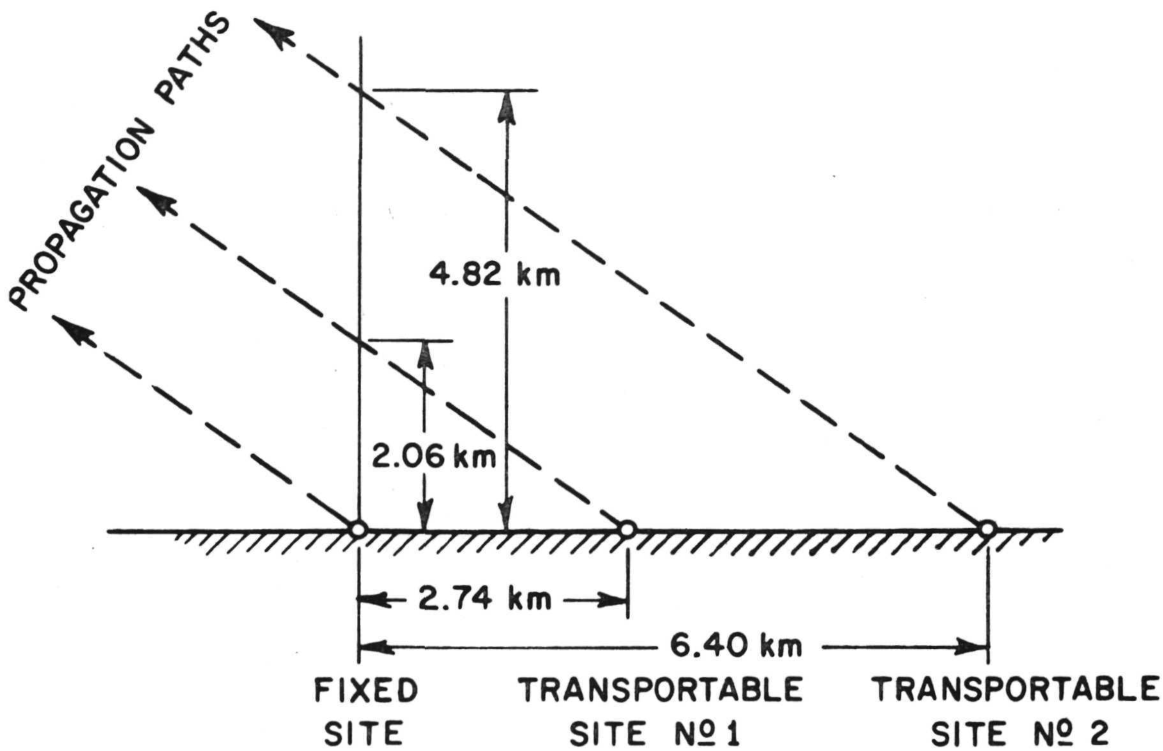

SITE	PATH SEPARATION		
	HORIZONTAL	VERTICAL	SPATIAL
Nº 1	2.99 km	2.06 km	3.41 km
Nº 2	6.71 km	4.82 km	7.73 km

Fig. 6. Side view of site locations.

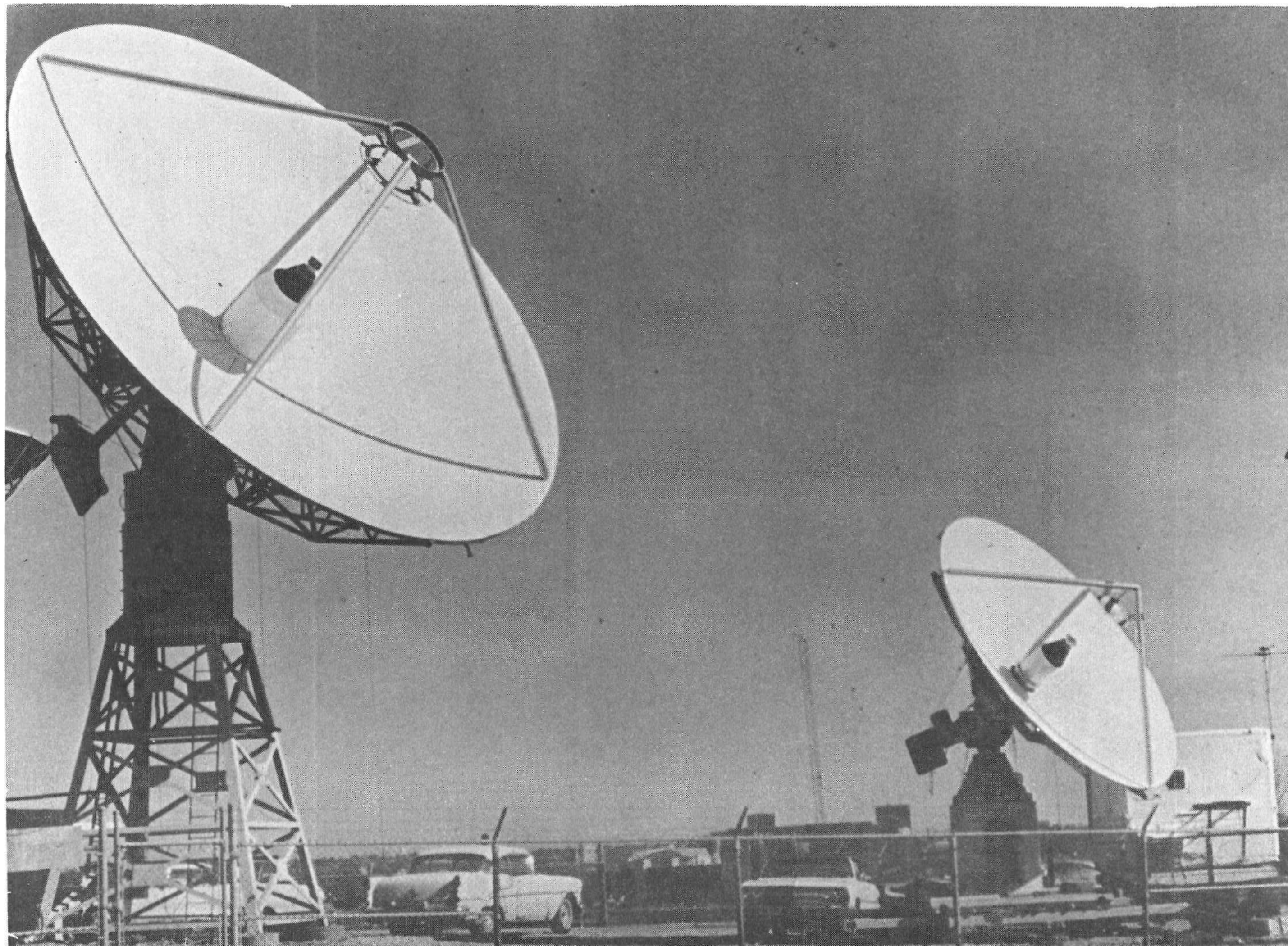

Fig. 7. Fixed and transportable antennas (1970).

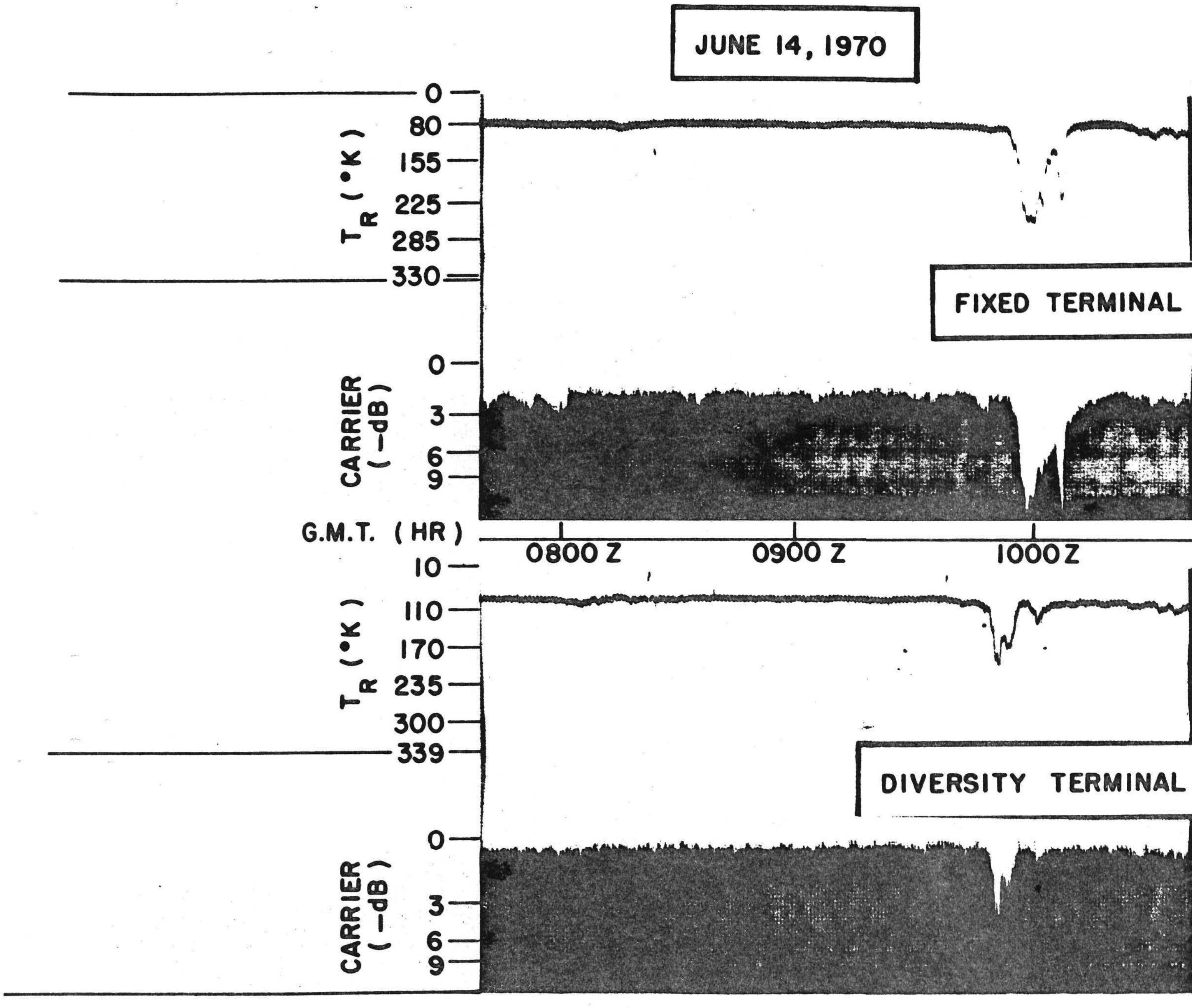

Fig. 8. Sample data at 4 km site separation.

detailed analysis of the data obtained using a separation distance of 4 km is contained in Reference 5.

A sample of the raw data obtained using the 8 km separation distance during 1971 is shown in Fig. 9. In this case a slowly moving cell produced a 13 dB fade at the fixed terminal while producing negligible attenuation at the transportable terminal. The increased signal level occurring at the fixed terminal at approximately 1715Z is a result of increasing the receiver gain by a factor of two.

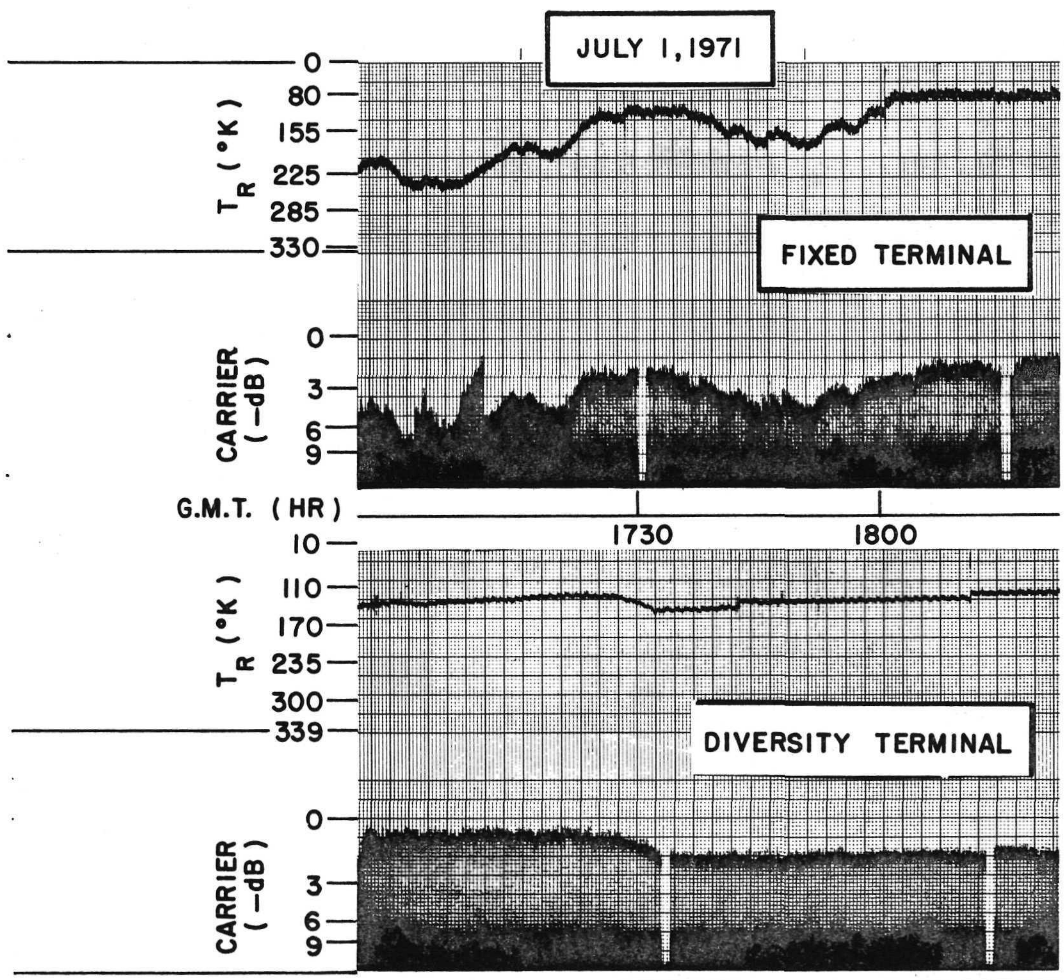

Fig. 9. Sample data at 8 km site separation.

For the purpose of studying the improvement resulting from space diversity operation, seven different storm events which produced significant fading were selected from the data obtained using the 4 km site separation for detailed analysis; nine such events were also selected from the data obtained using the 8 km separation distance. Treating each storm event individually, the cross-correlation between the attenuations observed at the two sites was calculated. A sample cross-correlation function for one storm event is shown in Fig. 10. Three characteristics of the storm event may be inferred qualitatively from this cross-correlation function. First, the time delay associated with the maximum of the cross-correlation function, in this case 8 minutes, is related to the speed with which the storm cell crosses the propagation paths. Second, the cross-correlation function evaluated for zero delay is an indicator of the effectiveness of a space diversity system operating in real time. And, third, the maximum value of the cross-correlation function is a measure of the change in the storm cell structure as it traverses through the two propagation paths, or, alternatively, the degree to which the propagation paths "slice" through different portions of the storm cell.

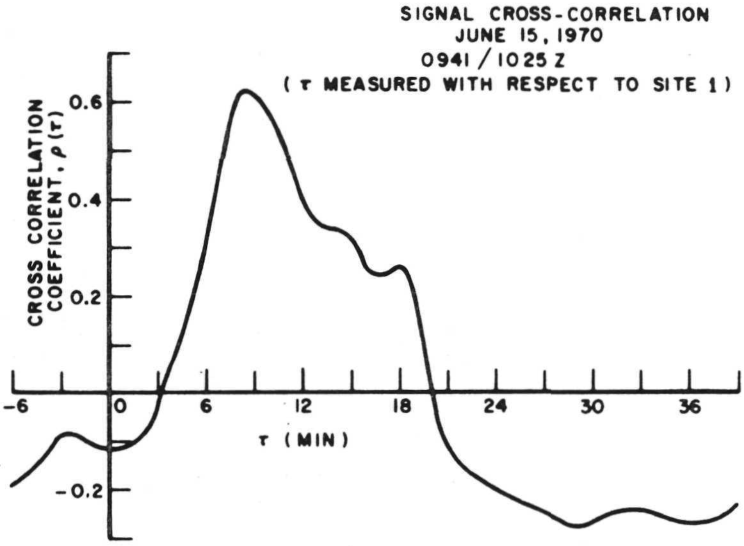

Fig. 10. Cross-correlation between receiver signals at two terminals separated by 4 km.

The cumulative cross-correlation functions for all the events analyzed in the two data periods were also calculated. The cumulative cross-correlation function at zero delay was 0.452 and the average delay time associated with the maximum cross-correlation function was 4.1 minutes for the data obtained using the 4 km terminal separation. Similarly, the cumulative cross-correlation function at zero delay was 0.268 and the average delay time of the maximum cross-correlation function was 10.2 minutes for the data using the 8 km terminal separation.

The fade distributions observed at the individual terminals as well as the fade distribution resulting from the space diversity mode of operation were also examined. These results for the 4 and 8 km separation distances are shown in Figs. 11 and 12, respectively. As expected, the individual terminal fade distributions are quite similar for the 4 km separation and show less similarity for the 8 km separation. The diversity fade distributions, labeled "BOTH" in the figures, were obtained by digitally comparing the individual terminal received signal records and selecting the larger signal on a second-by-second basis. This method of analysis corresponds to a simple switched diversity system operating in real time. Significant improvements in system performance would have resulted from the diversity mode of operation for both separation distances.

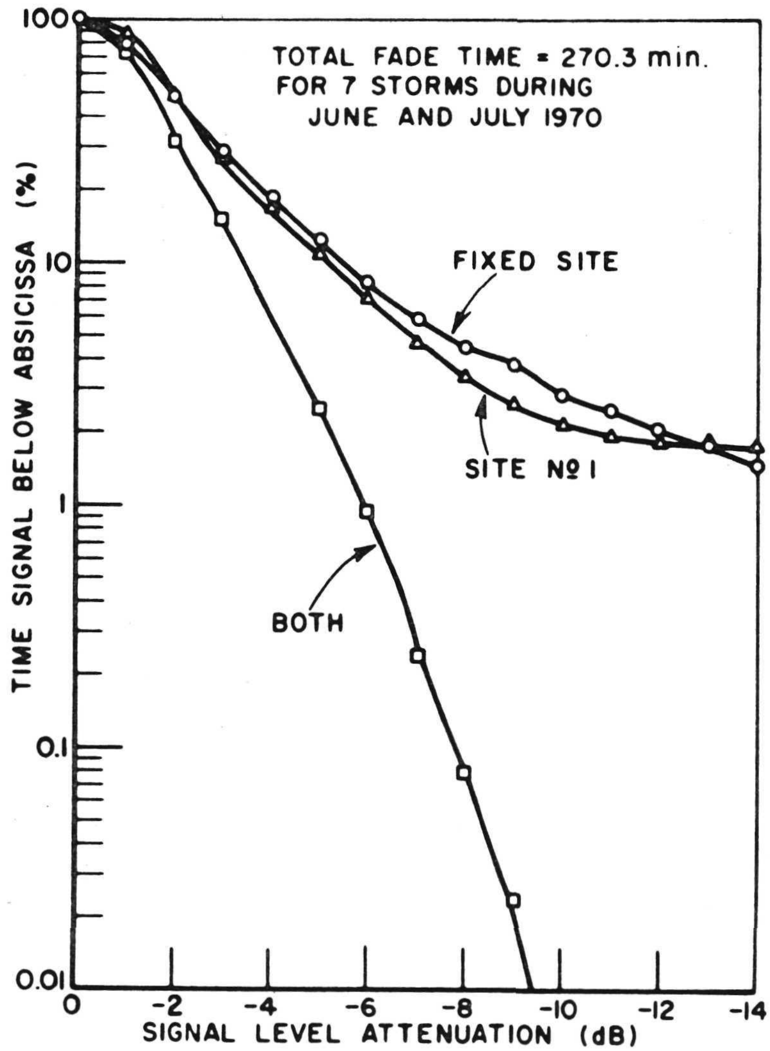

Fig. 11. Fade distributions for 4 km data.

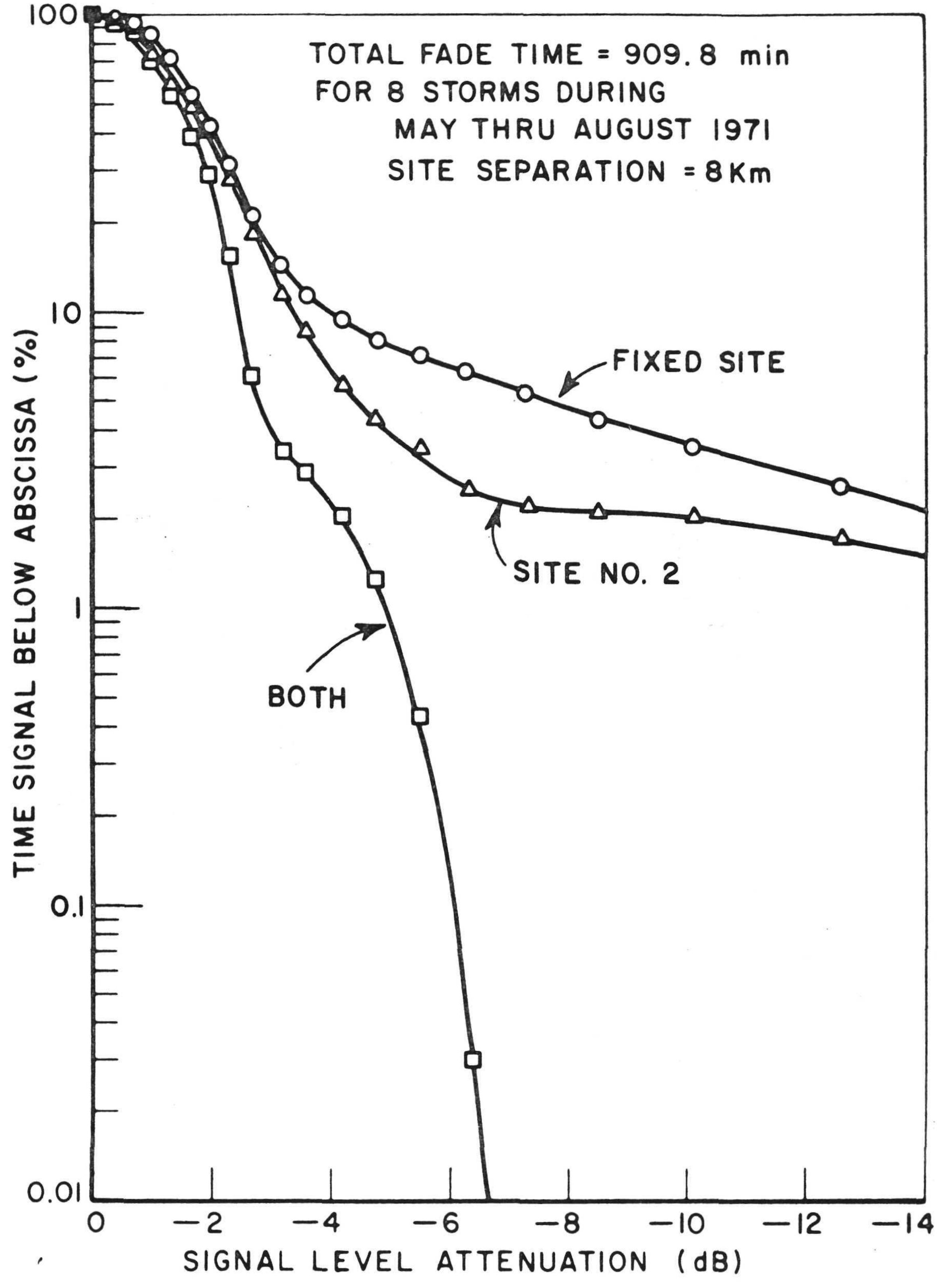

Fig. 12. Fade distributions for 8 km data.

Diversity gain may be defined as the difference between the signal level resulting from the diversity mode of operation and the median of the individual terminal received signal levels, both evaluated at a given percentage of occurrence. The diversity gain then corresponds to the improvement derived from diversity operation as compared to single terminal operation over a long period of time. Diversity gain data for both the 4 and 8 km separation distances as a function of single terminal fade depth are shown in Fig. 13. Note that the abscissa itself corresponds to diversity operation with zero separation, and the straight line with unity slope through the origin corresponds to ideal case where diversity operation eliminates all fading. Obviously, then, the 4 and 8 km diversity data must lie between these two limiting cases. Note, also, that the experimental data fall very nearly on straight lines having approximately unity slopes for fade depths exceeding 10 dB for the 4 km separation and 4 dB for the 8 km separation. This characteristic indicates that the diversity system is operating very much like an ideal system for fade depths below these levels and is, indeed, quite effective in improving system performance during periods of deep fading. Further examination of the diversity gain data indicates that the use of larger terminal separation distances will provide proportionally less improvement in system performance. This reduced degree of

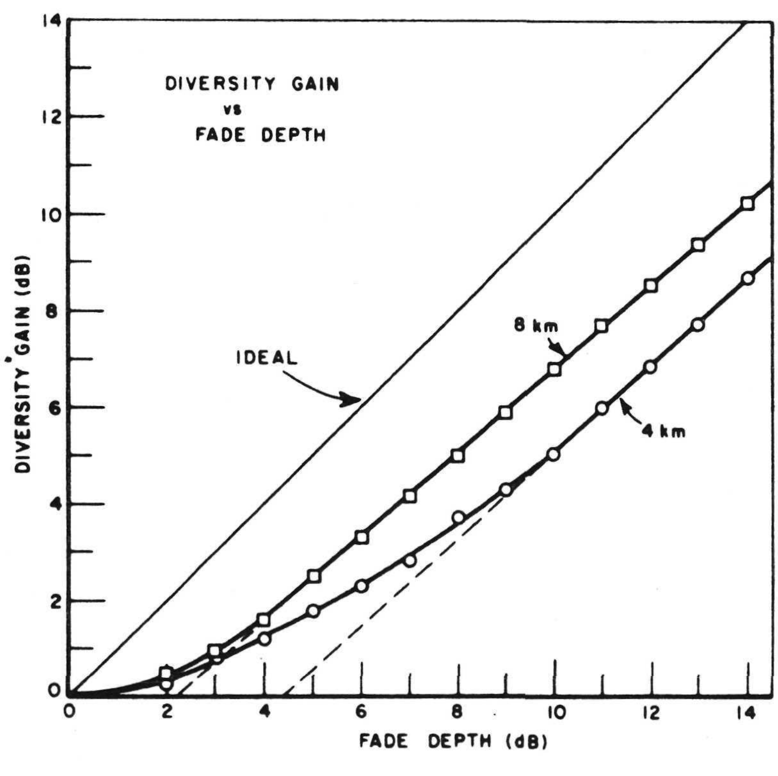

Fig. 13. Diversity gain versus single terminal fade depth.

improvement will also be purchased at the increased cost of the data link between the two ground terminals required for real time diversity operation. Another factor which will come into play as the separation distance is increased is fading due to the simultaneous intersection of the propagation paths by two different storm cells. PPI radar observations during the data gathering periods have indicated qualitatively that the events observed at the 4 and 8 km separation distances were completely dominated by single cells influencing both paths simultaneously.

In summary, data obtained using the ATS-5 15.3 GHz down-link have shown that significant system performance improvement results from the use of diversity receiving terminals spatially separated by 4 and 8 km. The durations of fades in excess of 10 and 6 dB, respectively, were reduced by at least two orders of magnitude in central Ohio. Further performance improvements to be gained by utilizing larger separation distances must be weighed against the increased costs of the data link between the ground terminals and the reduction in effectiveness resulting from the increased likelihood of fading produced by two different storm cells. Additional problems which remain to be examined include: the dependence of diversity gain upon a wider range of separation distances, the dependence of diversity gain upon the orientation of the separation baseline, and the dependence of both of these characteristics upon the meteorological environment encountered at various geographical locations.

REFERENCES

1. Freeny, A.E. and Gabbe, J.D., "A Statistical Description of Intense Rain," Bell System Technical Journal, V. 48, July 1969, p. 1789.

2. Semiannual Status Report, "Millimeter-Wavelengths Propagation Studies," Report 2374-3, 15 April 1969, ElectroScience Laboratory, The Ohio State University Department of Electrical Engineering, prepared under Grant NGR 36-080-008 for National Aeronautics and Space Administration, Washington, D.C. (N69-27155)

3. Semiannual Status Report, "Millimeter-Wavelength Propagation Studies," Report 2374-4, 30 April 1970, ElectroScience Laboratory, The Ohio State University Department of Electrical Engineering, prepared under Grant NGR 36-080-008 for National Aeronautics and Space Administration, Washington, D.C.

4. Hodge, D.B., Semiannual Status Report, "Millimeter-Wavelengths Propagation Studies," Report 2374-8, January 1972, ElectroScience Laboratory, The Ohio State University Department of Electrical Engineering, prepared under Grant NGR 36-080-008 for National Aeronautics and Space Administration, Washington, D.C.

5. Grimm, K.R. and Hodge, D.B., "A 15.3 GHz Satellite-to-Ground Diversity Propagation Experiment Using a Terminal Separation of 4 Kilometers," Report 2374-7, December 1971, ElectroScience Laboratory, The Ohio State University Department of Electrical Engineering, prepared under Grant NGR 36-080-008 for National Aeronautics and Space Administration, Washington, D.C.

THE ESTIMATION OF ATTENUATION STATISTICS FOR EARTH-SPACE MILLIMETER WAVELENGTH PROPAGATION

Logan R. Zintsmaster

ABSTRACT

The attenuation probability distributions for a millimeter wavelength earth-space propagation path are estimated for a single site and for a diversity configuration. The precipitation attenuation phenomenon is modeled by a cylindrical storm cell having a homogeneous rain rate. The attenuation probability distributions are then calculated from this storm cell model in terms of the rain rate probability density function, the cell diameter as a function of rain rate, and a fixed cell height. A rain rate probability density function which can be related to National Weather Service rain rate measurements is used in the calculations. Data from ATS-5 measurements for single sites in Rosman, North Carolina, and Columbus, Ohio, are compared to results calculated using typical storm parameters. In addition diversity calculations are compared with ATS-5 diversity measurements in Columbus, Ohio.

Precipitation in the form of rain is one of the major factors influencing the propagation of millimeter wavelength signals. One means used to characterize this effect is the attenuation probability distribution function. The ATS-5 experiment has been used to empirically measure this function and a need exists for a method to predict this function. This paper presents such a technique using a storm cell model for calculating the attenuation probability distribution from tipping bucket rain rate data. This model may also use tipping bucket rain data published by the National Weather Service.

In calculating the attenuation probability distribution the assumption was made that the precipitation events affecting the propagation of millimeter wavelength signals could be represented by cylindrical storm cells as shown in Fig. 1.

The storm cell is filled homogeneously with a rain rate r and has a fixed height, h. The diameter, a function of the rain rate r, represents an effective cell diameter. The location of the storm cell will be determined by the point where the vertical axis of the cell passes through the x,y plane. This point is identified as (x_0, y_0) and will be referred to as the center of the storm cell. The earth terminal,

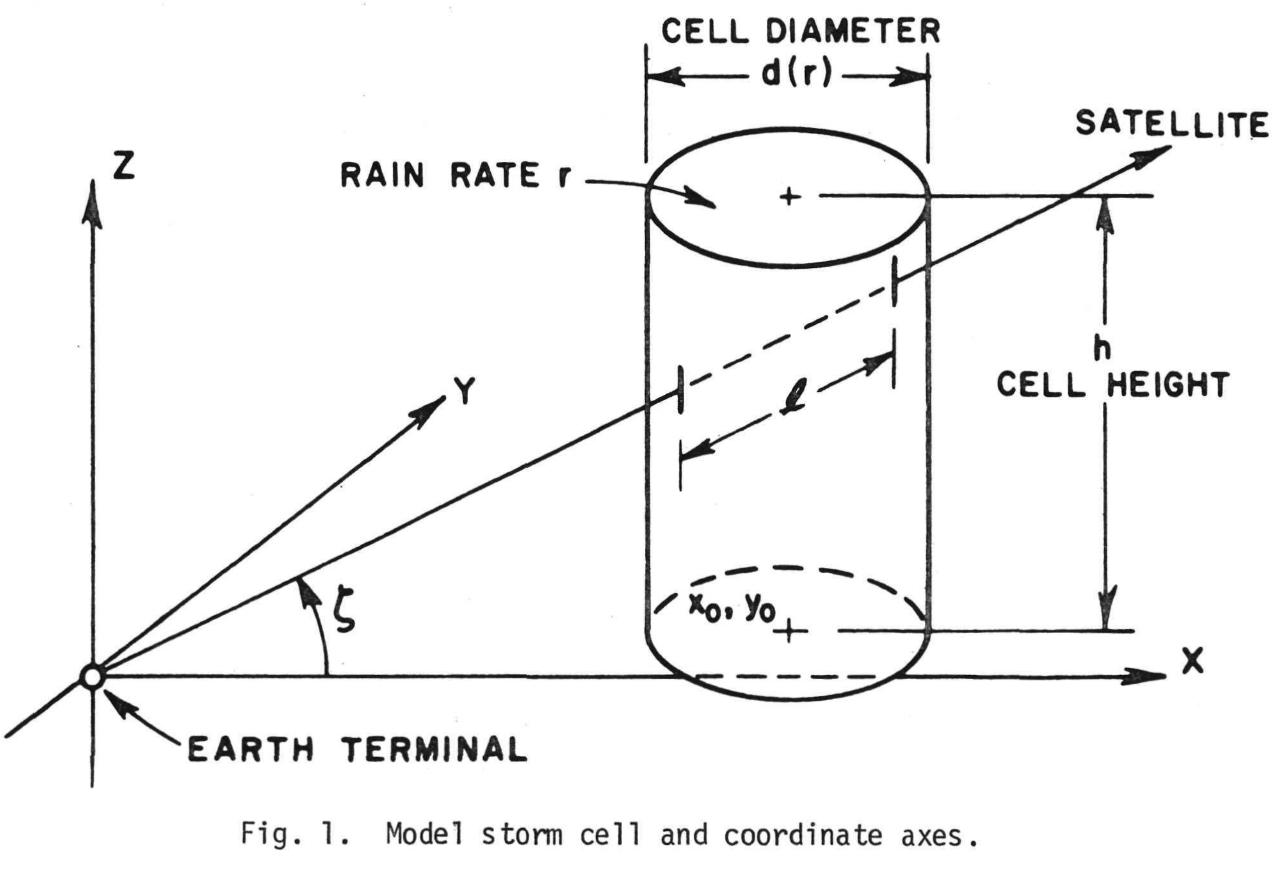

Fig. 1. Model storm cell and coordinate axes.

the propagation path and the coordinate axes are also shown. It is assumed that the terminal is located at the origin and that the propagation path lies in the x-z plane. The usual flat earth assumption has also been made.

There are four ways in which the storm cell may intersect the propagation path. In the first case, shown here, the propagation path enters the side of the cell and exits through the side. The length of the intersected path is shown as ℓ.

The other three types of intersections are:

1) The propagation path enters the side and exits through the top,

2) The path originates within the cell and exits through the top, and

3) The path originates within the cell and exits through the side.

In each of these four cases, the attenuation caused by the storm cell precipitation can be determined from the length of the intersected path, ℓ, and the storm cell rain rate, r, using the Gunn-East relation,

$$\text{(1)} \qquad \alpha = .035\, \ell\, r^{1.10} \quad .$$

The constants used here were interpolated from results calculated by Crane[1] from rain drop distribution measurements. In calculating the attenuation distribution the probability of a storm cell being centered at any point was assumed to be uniform over the universe of cell locations. Using the Gunn-East equation to relate the random variables α, r and ℓ, the attenuation probability distribution function was calculated and is

$$\text{(2)} \qquad P_\alpha(\alpha_0) = N \int_{r_{min}(\alpha)}^{\infty} [p_B(r) + p_{B0}\, \delta(r)]\, A(\ell_1(\alpha_0, r))/A_B(r)\, dr \cdot$$

This equation relates the attenuation distribution function to the tipping bucket rain rate probability density function and two areas which are functions of the cell geometry and the propagation path geometry. The constant N is used to normalize the equation so that P(0) = 1.

The first term in the integrand, the tipping bucket rain rate probability density function, has two parts. The first, $p_B(r)$ is the probability density that a non-zero rain rate is measured by the tipping bucket. The second, p_{Bo}, is the probability that a zero rain rate is measured. These functions account for the precipitation characteristics at the site being considered.

The functions which depend on the cell geometry are $A_B(r)$ and $A(\ell_1(\alpha_o,r))$. $A_B(r)$ is the area within which a storm center may be located and produce rainfall into the tipping bucket. The function $A(\ell_1(\alpha_o,r))$ is the area within which a storm center may be located and intersect the propagation path over a length greater than or equal to ℓ_1.

Since the storm cell has a finite maximum diameter, there is a maximum possible intersected path length for a given attenuation, α_o. This requires that a minimum rain rate be present in the cell for that attenuation to occur. This minimum rain rate is $r_{min}(\alpha)$, the lower limit of the integration.

For the model to be of maximum usefulness the rain rate density function should reflect the precipitation characteristics of each terminal location being considered. Data for stations all over the United States are published by the National Weather Service, however, the rain rates which are measured are averaged over a one hour time interval and are too coarse to use directly in the calculation.

It has been found by Rice and Holmberg[2] that the tipping bucket probability distribution function could be approximated by the sum of three exponential functions called modes. It was further found that the modes for different averaging times were related so that given the mode parameters for a particular averaging time the corresponding mode parameters for a different averaging time could be calculated.

From this distribution, the tipping bucket rain rate density function for non-zero rain rates was calculated and is shown in Eq. (3).

(3) $$p_B(r) = \sum_1^3 A_i/B_i \exp(-r/B_i) \quad .$$

The mode coefficient, A_i, will be calculated from measured rain rate data. The mode rates, B_i, used are taken from the Rice-Holmberg calculations. The zero rain rate probability is determined from Eq. (3) and is given below.

(4) $$p_{BO} = 1 - \sum_1^3 A_i \quad .$$

To include the precipitation characteristics of a particular site into the attenuation distribution the hourly precipitation data published by the National Weather Service is used to calculate a best fit Rice-Holmberg clock-hourly rain rate distribution function. From this function the clock one minute distribution function is calculated.

Although it would be ideal to have the instantaneous statistic the clock one minute statistic is the best presently available.

The other terms in the integrand are functions of the storm cell and propagation path geometry . The area within which a storm cell can be located and rain in the tipping bucket rain gauge, $A_B(r)$, is a circular region, centered at the tipping bucket. This area is $\pi(d(r))^2/4$. The area within which a storm cell may be centered and intersect the propagation path is shown in Fig. 2 for the single and two site calculations. For a single site the region is centered about the x-axis and represents the area where a storm cell may be centered and intersect the path over a length greater than or equal to $\ell_1(\alpha_0,r)$. To calculate the two site joint attenuation distribution, the storm cell must intersect both propagation paths simultaneously. Thus, the path intersection area $A(\ell_1(\alpha,r)$ is the area of overlap of the two single site intersection areas. The analytic forms of these areas is determined in a straight forward manner from the storm cell-propagation path geometry.

Having calculated the attenuation probability distribution function for the model storm cell, the storm cell dimensions, h and d(r), must now be related to the physical precipitation process so that calculations can be made. The cell height, h, represents the height of the precipitation cell. For most of the United States a value of 5 to 7 km is typical. It has been found that the results are not very sensitive to the exact choice so an average of 6 km was used in the calculations presented here.

Whereas the cell height corresponds to the physical height of a rain cell, the storm cell diameter represents an effective diameter and thus may not correspond well with the actual physical dimensions of rain cells. Several proposed diameter-rain rate functions are shown in Fig. 3.

The first is a modified form of the CCIR function. The original function becomes negative for rain rates greater than about 50 mm/hr. Since this does not seem realistic, the function was modified so that the minimum cell diameter was clamped to 1.25 km. The choice of the minimum diameter was based on data from Bell Labs suntracker measurements presented by Hogg[3]. An exponential function was fitted to Hogg's data for use in numeric calculations and is also shown in this figure.

The third diameter function shown was determined empirically from the 1970 Ohio State University ATS-5 data using the mode concept presented by Rice and Holmberg. Since the Rice-Holmberg distribution characterizes different types of precipitation processes in terms of three modes, it seemed logical to characterize the size of these precipitation cells in a modal form also. For the calculations to be presented here, the Bell fit diameter function and the three mode diameter function were used.

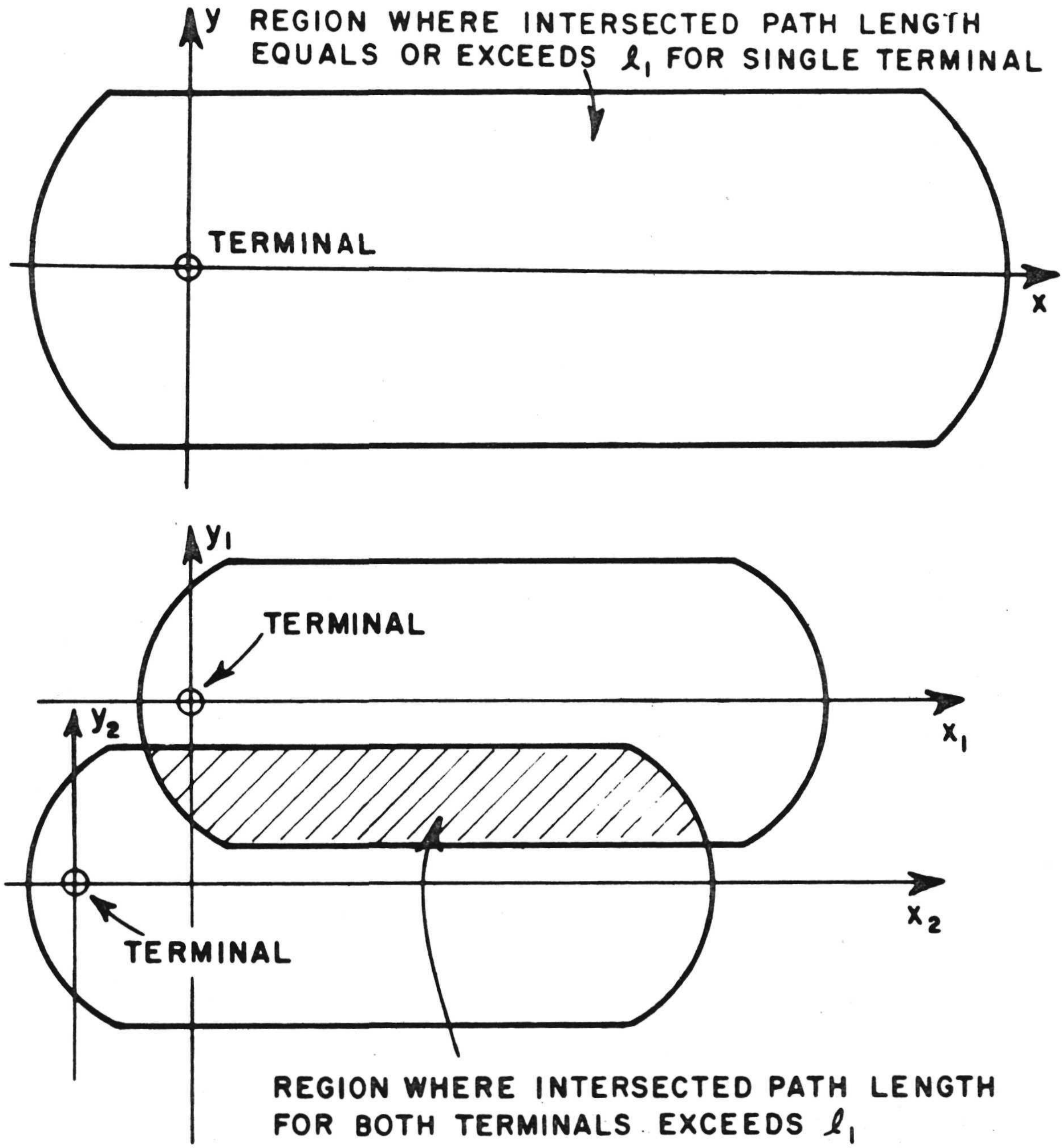

Fig. 2. Areas of storm cell center locations for propagation path intersections with one and two terminals.

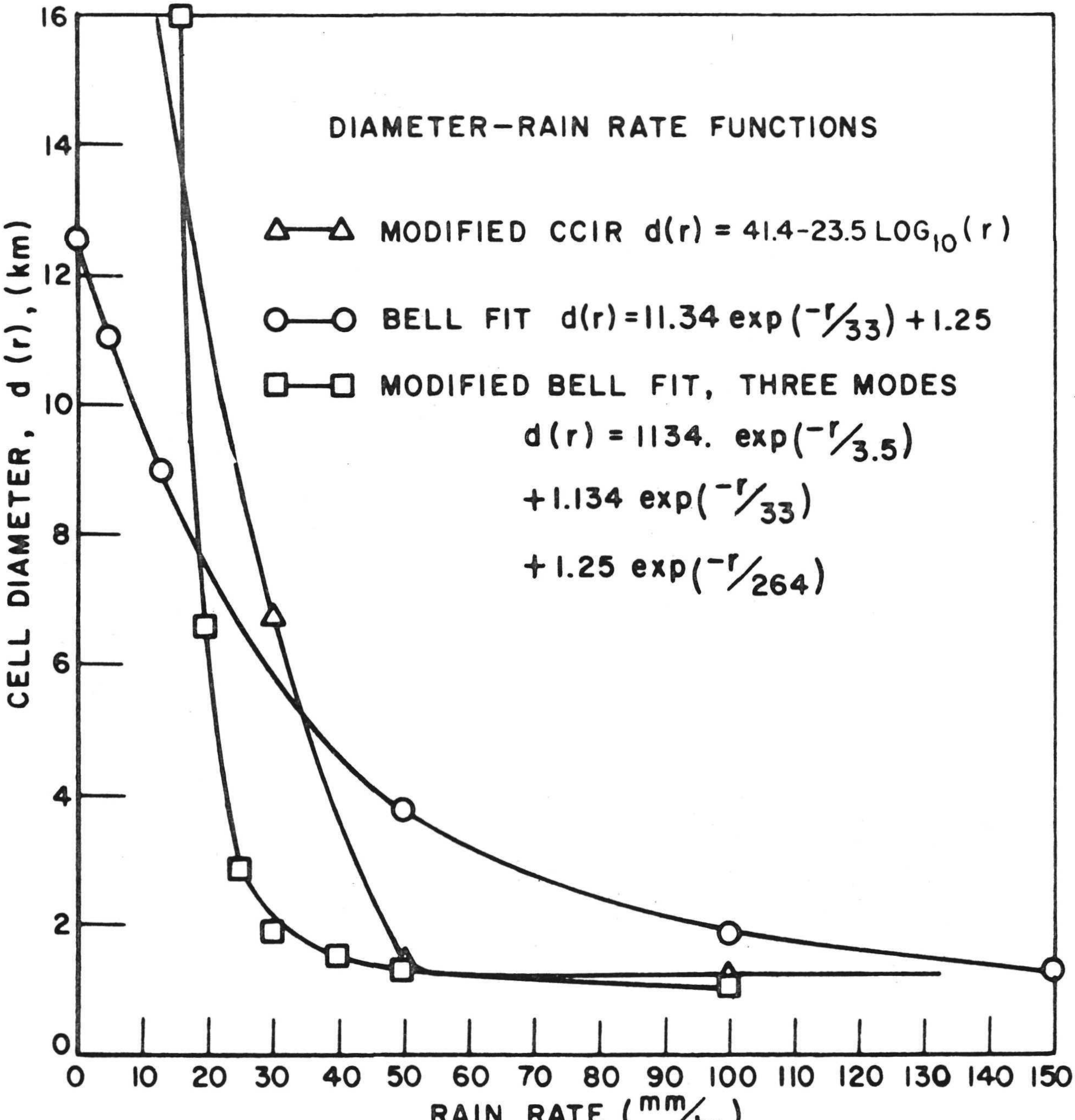

Fig. 3. Diameter-rain rate models.

In order to make a fair comparison between the calculated attenuation distribution and the measured attenuation distribution, the rain rates which occurred during the attenuation measurements were used to calculate the A_i's in the Rice-Holmberg distribution. A comparison of the best fit Rice-Holmberg distribution and the rain rates measured at NASA Rosman in 1970 are shown in Fig. 4. It is seen here that the Rice-Holmberg distribution fits the data very well.

Using this rain rate distribution and the Bell fit diameter function the attenuation distribution for the NASA Rosman terminal was calculated and is shown in Fig. 5. The error criterion which is used to evaluate the comparison of the measured and calculated results is the horizontal distance between the curves. This criterion gives the attenuation difference between the calculated and experimental attenuation for a constant probability. It can be seen that the calculated distribution brackets the measured distribution. For low attenuations the results are about 3 dB low. For high attenuations the calculated distribution is about 3 dB high.

Using the three mode diameter function the results were improved significantly as shown in Fig. 6. The error at low attenuations has been reduced to 2 dB and at high attenuations the error is only .5 dB. It is seen that the calculated distribution agrees well with the measured distribution.

As mentioned earlier the three mode diameter function was found by fitting the calculated attenuation distribution to the single site distribution measured at Ohio State in 1970. This fit is shown in Fig. 7. The flattening of the measured curve was ignored in the fit since it resulted from margin limitations in the measurements.

In Fig. 8 the storm cell model was used to calculate the two terminal joint attenuation distribution for the 4 km spacing used in 1970 at Ohio State University. It is seen here that good agreement is also obtained.

To summarize the results using the three mode diameter function the error curves were calculated and are shown in Fig. 9. It is seen that the three mode diameter function gives good agreement with the 1970 experimental data.

In conclusion, the single site attenuation distribution and the two site joint attenuation distribution were calculated using a cylindrical storm cell model. A technique was described for using National Weather Service precipitation data to calculate the attenuation distribution for a particular site location. Using a three mode diameter function it was shown that the model agreed within 2 dB for both the single site attenuation distribution and the two site joint attenuation distribution when compared with ATS-5 propagation measurements. Although this storm cell model represents a first attempt at making this type of calculation it appears to be a promising approach and provides a basis for future model development.

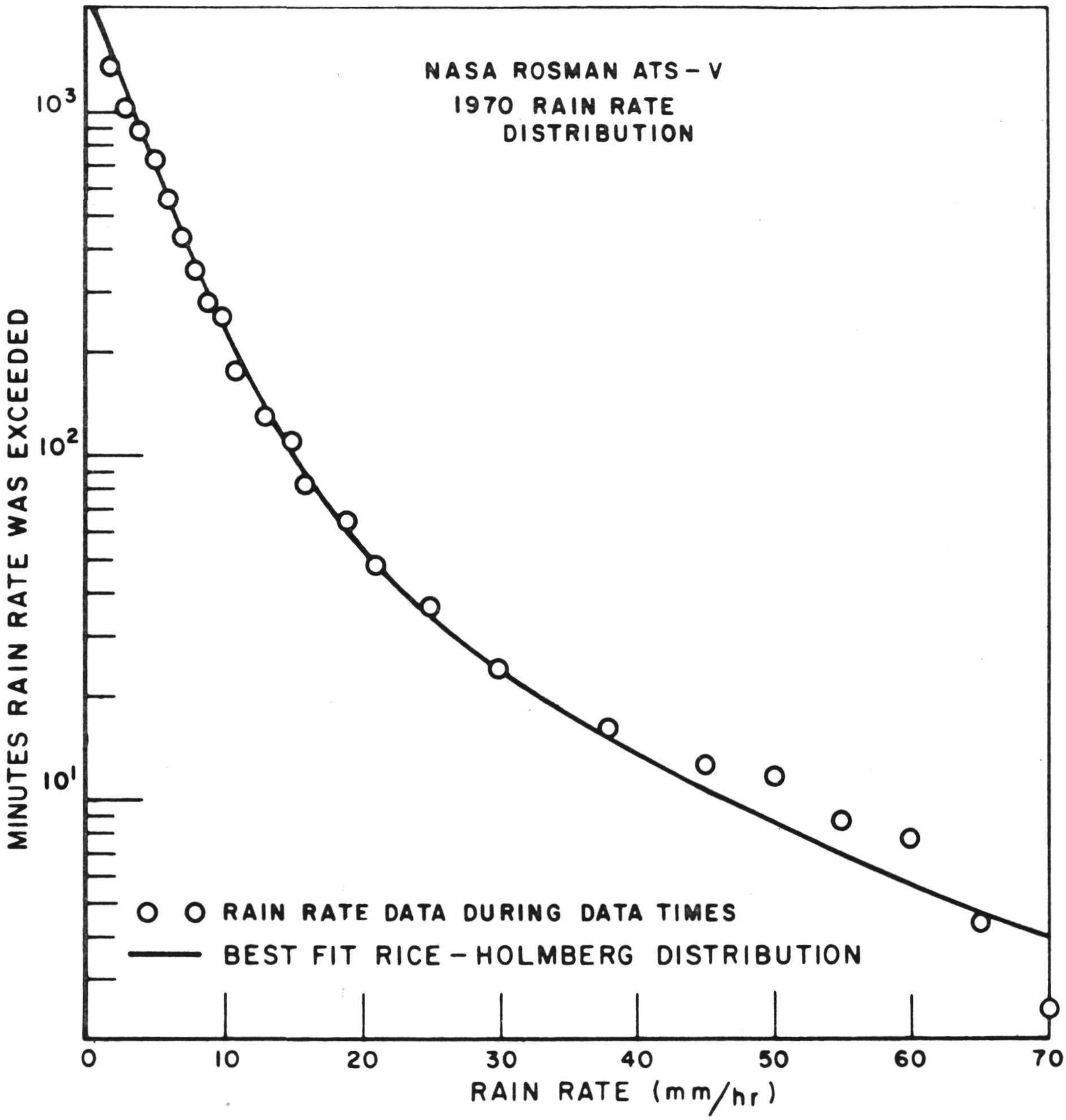

Fig. 4. NASA Rosman rain rate data.

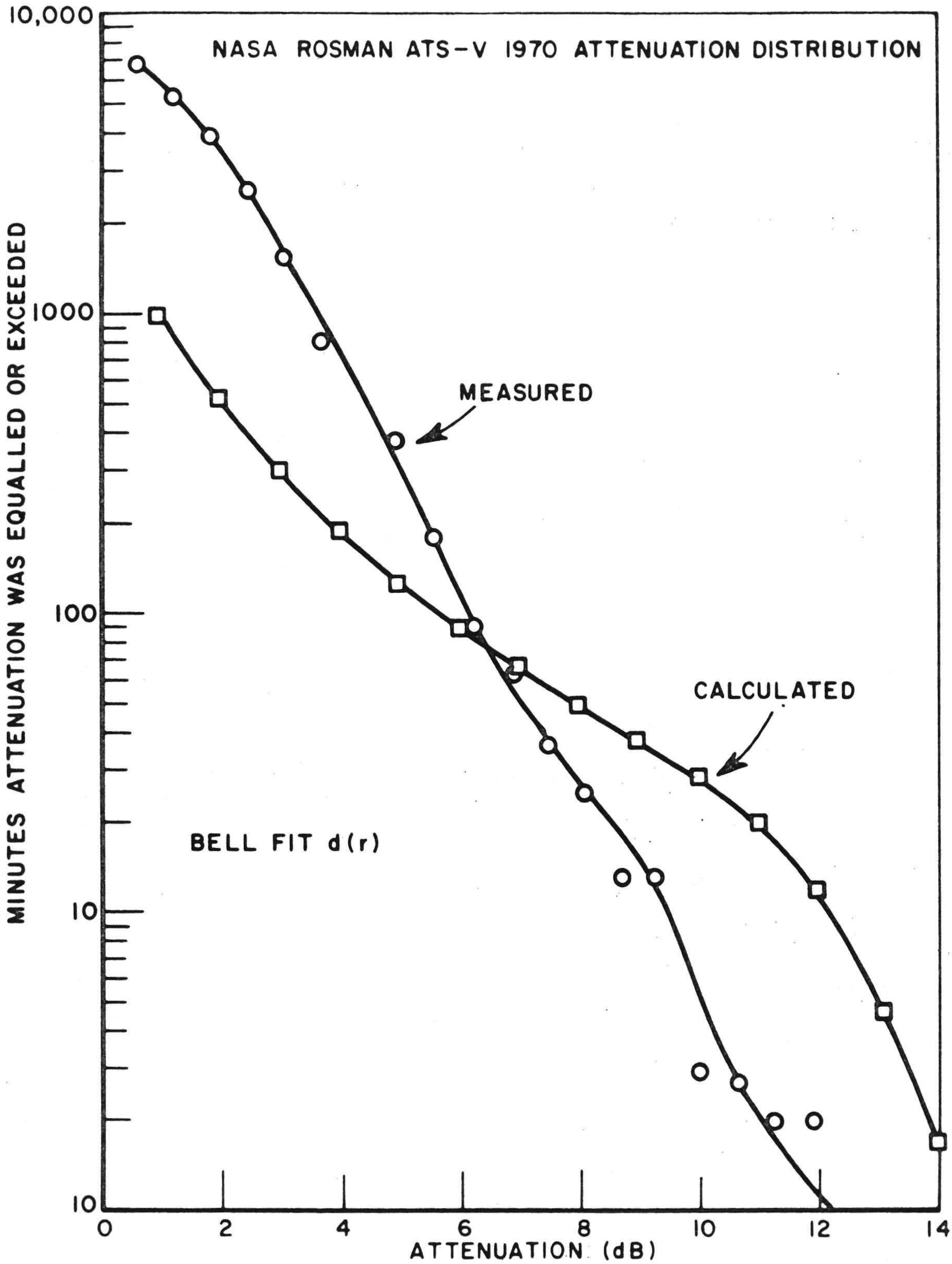

Fig. 5. Calculated NASA Rosman fade distribution using exponential diameter model.

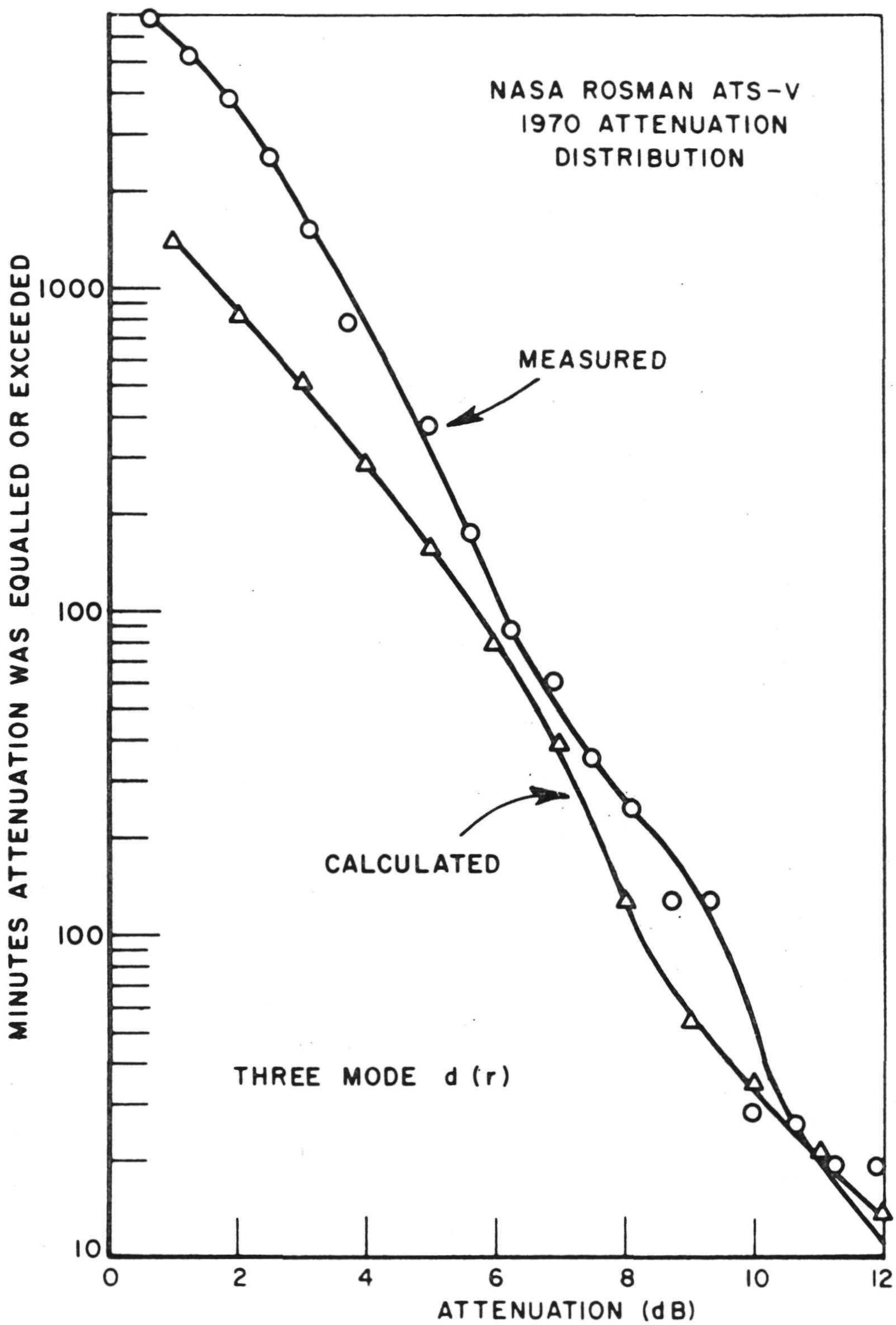

Fig. 6. Calculated NASA Rosman fade distribution using 3 mode diameter model.

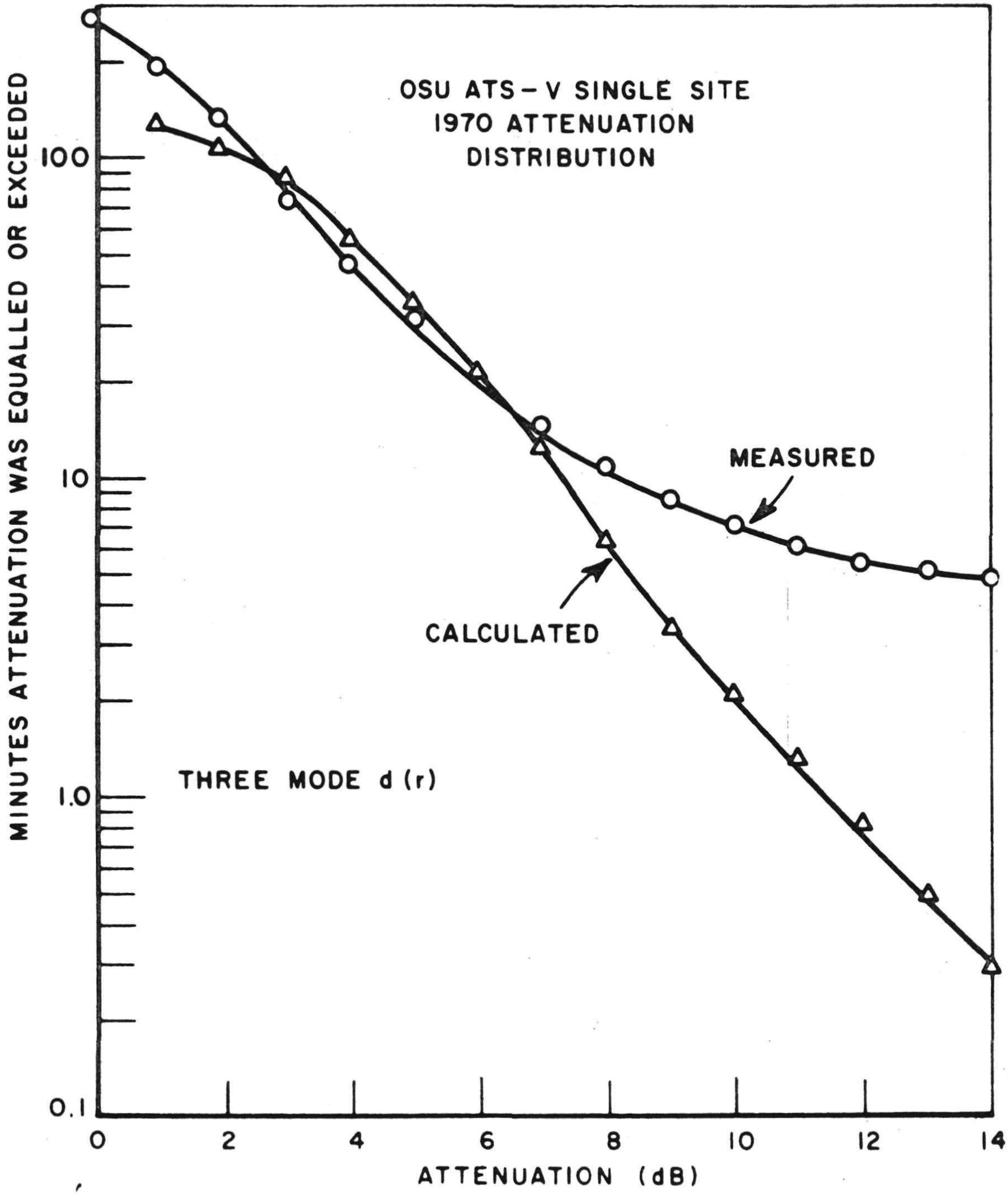

Fig. 7. Calculated OSU single terminal fade distribution using 3 mode diameter model.

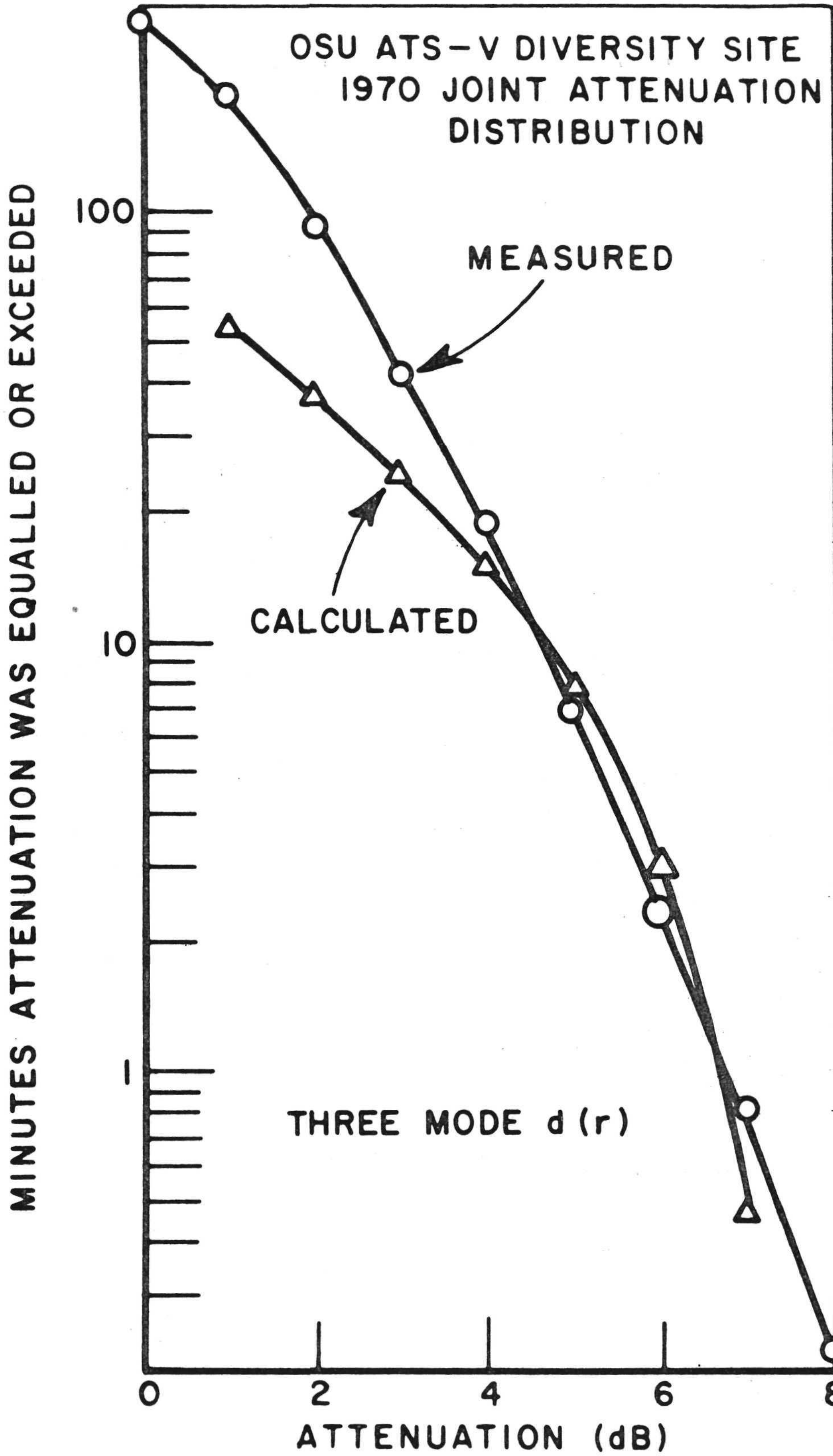

Fig. 8. Calculated OSU diversity fade distribution using 3 mode diameter model.

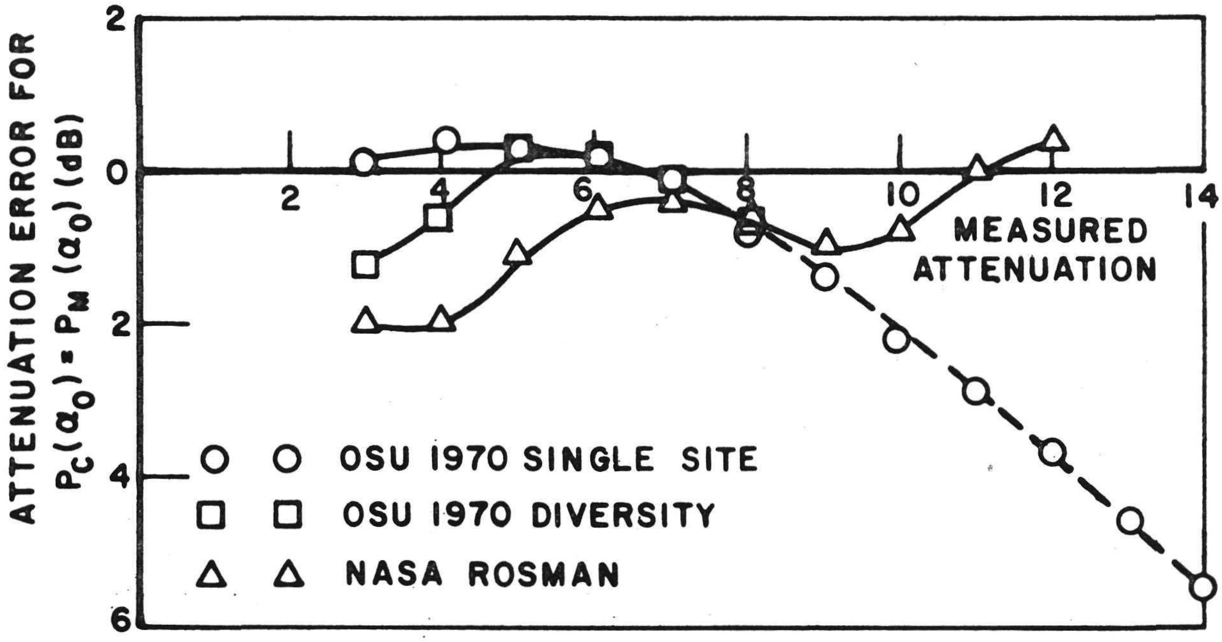

Fig. 9. Attenuation prediction error for storm cell model.

REFERENCES

1. Crane, R.K., "Propagation Phenomena Affecting Satellite Communication Systems Operating in the Centimeter and Millimeter Wavelength Bands," Proc. IEEE, 59, 1971, pp. 173-188.

2. Rice, P.L. and Holmberg, N.R., Private Communication, ITS Laboratories, Boulder, Colorado, 1971.

3. Hogg, D.C., "Rain on Earth-Space Paths," 1971 G-AP International Symposium.